Pyrocumulonimbus Events over British Columbia in 2017: An ensemble model study of parameter sensitivities and climate impacts of wildfire smoke in the stratosphere

Hsiang-He Lee*, Katherine A. Lundquist, and Qi Tang

Lawrence Livermore National Laboratory, Livermore, CA, U.S.A.

Submitted to
Journal of Geophysical Research – Atmosphere

April 2022

*Corresponding author address: Dr. Hsiang-He Lee, 7000 East Avenue, Livermore, CA, 94550, U.S.A.

E-mail: lee1061@llnl.gov

Key points:

- An ensemble study of E3SM simulations determines the best combination of smoke parameters to match observations from the 2017 PyroCb events.
- The Random Forest technique is used to quantify the relative importance of parameter and finds the greatest sensitivity to injection height.
- The lifetime of stratospheric smoke from the 2017 PyroCb events is similar to the observations, about ~180 days.

Abstract

Pyrocumulonimbus (pyroCb) are fire-triggered or fire-augmented thunderstorms and can by transporting a large amount of smoke particles into the lower stratosphere. With satellite remote sensing measurements, the plumes from pyroCb events over British Columbia in 2017 were observed in the lower stratosphere for about 8-10 months after the smoke injections. Several previous studies used global climate models to investigate the physical parameters for the 2017 pyroCb events, but the conclusions show strong model dependency. In this study, we use Energy Exascale Earth System Model (E3SM) atmosphere model version 1 (EAMv1) and complete an ensemble of runs exploring three injection parameters: smoke amount, the ratio of black carbon to smoke, and injection height. Additionally, we consider the heterogeneous reaction of ozone and primary organic matter. According to the satellite daily observed aerosol optical depth, we find that the best ensemble member is the simulation with 0.2 Tg of smoke, 2% of which is black carbon, a 13.5 km smoke injection height, and a 10^{-6} probability factor of the heterogenous reaction of ozone and primary organic matter. We use the Random Forest machine learning technique to quantify the relative importance of each parameter in accurately simulating the 2017 pyroCb events and find that the injection height is the most critical feature. Due to the long lifetime and wide transport of stratospheric aerosols, the estimated e-folding time of smoke aerosols in the stratosphere is about 178 days, and the global averaged shortwave surface cooling is -0.334 W m^{-2} for about 10 months.

Plain Language Summary

Pyrocumulonimbus (pyroCb) caused by extreme wildfires can transport a large amount of smoke particles into the lower stratosphere, which then affects the climate. Several previous studies used global climate models, along with satellite observations of smoke, to investigate the injection parameters for 2017 pyroCb events over British Columbia, but the conclusions show strong model dependency. This study uses the Energy Exascale Earth System Model (E3SM) atmosphere model version 1 (EAMv1) and completes an ensemble of simulations targeting three loosely constrained injection parameters: smoke amount, the ratio of black carbon to smoke, and injection height. Additionally, we consider the heterogeneous reaction of ozone and primary organic matter in the ensemble model. We use the Random Forest machine learning technique to quantify the importance of each parameter in accurately simulating the 2017 pyroCb event. Finally, a model simulation with the best combination of injection parameters shows the estimated smoke lifetime in the stratosphere is about 178 days, and a global-averaged shortwave surface cooling of -0.334 W m^{-2} for about 10 months.

Keywords:

E3SM, wildfire, Pyrocumulonimbus, stratospheric aerosols, machine learning, aerosol radiative effects

1 Introduction

In recent years, extreme wildfires have frequently occurred in the western United States and Canada. Pyrocumulonimbus (pyroCb) are fire-triggered or fire-augmented thunderstorms and can transport a large amount of smoke particles into the lower stratosphere (Fromm et al., 2005; Fromm et al., 2010). Aerosols in the lower stratosphere from volcanic eruptions and large wildfires have been detected and monitored with the modern satellite remote sensing observations in the past decades (Fromm et al., 2000; Peterson et al., 2018; Vernier et al., 2009).

PyroCb and volcanic eruptions are important geophysical extreme events because they can perturb the stratospheric aerosol loading for several months and have substantial climate impacts locally and globally. The smoke aerosols injected into the stratosphere from pyroCbs mainly contain black carbon (BC) and organic carbon (OC) aerosols (Andreae, 2019; Andreae & Merlet, 2001; Park et al., 2003) and have different radiative effects from the sulfate aerosols released by volcanic eruptions. Volcanic sulfate aerosols have a strong cooling effect due to scattering. With carbonaceous aerosols, BC absorbs shortwave radiation, while particulate organic matter scatters it, which leads to atmosphere warming and surface cooling (Bergstrom et al., 2002; Malone et al., 1985). Additionally, through the absorption of solar radiation and subsequent heating, BC can self-loft, lengthening its atmospheric lifetime. In the 1980s, Malone et al. (1985) used a three-dimensional circulation model to simulate injected smoke in the atmosphere that might be introduced by a nuclear war. They concluded that the heating from BC shortwave absorption gives rise to vertical motions that carry smoke above the original injection height around the tropopause. Later, the changes of solar heating profile due to BC absorption were supported by the measurements of the field campaign, High-performance Instrumented Airborne Platform for Environmental Research Pole-to-Pole Observations (HIPPO), between early 2009 and mid-2011

(Schwarz et al., 2013). Thus, the radiative effects of the pyroCb injected smoke in the stratosphere can be very important in the global radiation budget.

Several previous studies used satellite observations and global climate models (GCMs) to investigate the injection parameters for 2017 pyroCb events over British Columbia, but the conclusions show strong model dependency (Christian et al., 2019; Das et al., 2021; Yu et al., 2019). The pyroCb events occurring in British Columbia, Canada in August 2017 were considered the most extensive known stratospheric intrusion from pyroCb activity at that time. Based on the combination of lidar and passive remote sensing observations, Peterson et al. (2018) estimated the injected aerosol amount of 0.1-0.3 Tg, while Torres et al. (2020) projected around 0.18-0.35 Tg, by using three different satellite remote sensing observations, comparable to a moderately sized volcanic eruption (Ge et al., 2016; Hofmann et al., 2009; J. Wang et al., 2013). In previous studies, smoke injection height varies from 10 km (Das et al., 2021) to 13 km (Christian et al., 2019; Yu et al., 2019), and the ratio of BC to smoke ranges from 2% - 6%. GCM simulations in Christian et al. (2019) show that the pyroCb smoke particles cause radiative forcing of 0.02 W m^{-2} at the top of the atmosphere (TOA), averaged globally in the 2 months following the events; however, Das et al. (2021) saw -0.03 W m^{-2} global mean radiative forcing at TOA in the first month after the events. Both studies used the NASA Goddard Earth Observing System (GEOS) with a chemical transport model to conduct their simulations, but the model configuration were different.

Wagman et al. (2020) used the Department of Energy (DOE) Energy Exascale Earth System Model (E3SM) atmosphere model version 1 (EAMv1) to examine the climate impacts of massive urban fires in South Asia induced by a regional nuclear exchange scenario. The study found that uncertainties in the modeled aerosol radiative properties and smoke composition, particularly the percentage of BC and primary organic matter (POM) in the total aerosol mass,

propagate through to produce significant uncertainties in the climate response. In their study, overall climate impacts are comparable in initial magnitude (i.e., surface cooling), but have a much a shorter duration compared to previous assessments with the same smoke injection (Mills et al., 2014; Reisner et al., 2018).

In this study, we use EAMv1 with the CMIP6 (Coupled Model Intercomparison Project Phase 6) configuration, which is different from the CMIP5 used in Wagman et al. (2020), to assess the 2017 pyroCb event over British Columbia and perform an ensemble simulation targeting three important, yet uncertain fire smoke injection parameters: smoke amount, the ratio of black carbon to smoke, and injection height. Additionally, we consider the probability parameter (gamma) of the heterogeneous reaction of ozone and organic carbon suggested by Yu et al. (2019) in the ensemble experiments. The purpose of this study is to quantify the performance of the E3SM model in simulating the climate disturbance of a stratospheric wildfire smoke injection, when compared to observations. We also want to examine the lifetime of stratospheric smoke in EAMv1, and the magnitude and duration of the climate perturbation, to see if they agree with observations, as this would have important implications for studies of climate impacts due to a nuclear exchange, for example Wagman et al. (2020).

A brief description of EAMv1, simulation set-up, parameters for the ensemble study, and observational data are given in Section 2. Simulation results and discussion are shown in Section 3 and Section 4, respectively, with a summary provided in Section 5.

2 Methodology

2.1 Model description and configuration

The DOE E3SM coupled model version 1 was released to the community in April 2018. A detailed description is documented in Golaz et al. (2019). The overview of the atmosphere

component of E3SMv1, E3SM Atmosphere Model (EAMv1) is provided by Rasch et al. (2019). EAMv1 uses a spectral element dynamical core at a 110-km resolution (at equator) on a cubed sphere geometry and a traditional hybridized sigma-pressure vertical coordinate. The transition between terrain-following and constant-pressure coordinates is made at ~200 hPa (~11km). EAMv1 has 72 vertical layers with a model top at approximately 60 km (10 Pa).

EAMv1 uses the two-moment Modal Aerosol Module (MAM4), with four internally mixed lognormal size modes, to represent the size distribution and mixing state of aerosols (X. Liu et al., 2016). EAMv1 has several enhanced features in MAM4 (H. Wang et al., 2020). One important modification to MAM4 is that based on the original MAM3, the addition of freshly emitted primary carbonaceous aerosols (e.g., BC and POM) as a primary-carbon mode to treat the aging process of BC/POM, when combined with the three commonly defined size aerosol modes (Aitken, accumulation, and coarse mode). The transfer or "aging" of carbonaceous aerosols from the primary-carbon mode to the accumulation mode occurs after particles condense eight monolayers of (hydrophilic) sulfate, particles condense enough secondary organic aerosol (SOA) to change the volume-weighted hygroscopicity by the same amount as eight layers of sulfate, or particles coagulate with hydrophilic Aitken-mode particles.

The stratospheric ozone is simulated by the linearized chemistry version 2 (Linoz v2) (Hsu & Prather, 2009), which calculates the first-order Taylor expansion terms for the stratospheric ozone production and loss based on local temperature, local ozone abundance, and the overhead ozone column.

In this study, we choose the compset F2010C5-CMIP6-LR, which configures an atmosphere-only simulation using the CMIP6 forcing and prescribed sea surface temperature and sea ice with observed climatology. The initial condition of the model configuration is from an

E3SMv1 Atmospheric Model Intercomparison Project (AMIP) simulation (Golaz et al., 2019) on January 1, 2010. Monthly climatological emissions from 2005 to 2014 are used to generate background aerosols in the atmosphere. The default EAMv1 CMIP6 setup uses climatological volcanic aerosols' optical properties to calculate aerosol radiative effects in the stratosphere instead of explicitly calculating existing aerosol radiative effects, which are function of aerosol particle size and concentration. To study the impacts of the 2017 cyroCb event, we removed the CMIP6 pre-calculated volcanic aerosol radiative effects and added wildfire smoke as an extra aerosol source in the stratosphere. Note that in this study, the instantaneous radiative effects of stratospheric aerosols are diagnosed by performing two sets of radiative transfer calculations (i.e., double call), one with stratospheric aerosols only and the other without any aerosols in the model column, to calculate the flux differences.

2.2 Nudging for meteorological conditions

Nudging is a method of data assimilation to constrain the evolution of the prognostic variables to be similar to the evolution of those variables in a predefined reference simulation (e.g., reanalysis data). In general, only a small number of model variables are nudged, and other fields are allowed to evolve in response to the physical and dynamical processes in the model.

In order to provide more realistic meteorological conditions to facilitate the time-specific evaluations of fire simulations against observations, we nudge towards ERA-Interim data, which is a global atmospheric reanalysis from the European Centre for Medium-Range Weather Forecasts (ECMWF) (*ERA-Interim Project*, 2009) and provides 6-hourly U and V wind components, and temperature (T) for meteorology nudging. The simulation runs from January 1, 2017, to August 11, 2017, with the horizontal wind components and temperature nudged towards the ERA-Interim reanalysis data, following the setup in Yu et al. (2019), and using linear function

187 nudging (Sun et al., 2019; Tang et al., 2019) with a 50-hourly time frequency (i.e., relaxation time
188 scale). Starting from August 12, 2017, the day of the PyroCb event, the model runs freely without
189 nudging to the end of May of 2018 to simulate smoke transport and aerosol-radiation interactions.
190 The evaluation and discussion of the nudging time scale are in Section 3.1.

191 ## 2.3 Numerical experiments for the ensemble study

192 Previous studies demonstrated that three injection parameters: total smoke amount, the
193 ratio of black carbon to smoke, and injection height are critical for accurate simulation of the
194 smoke transport (Christian et al., 2019; Das et al., 2021; Yu et al., 2019). Additionally, Yu et al.
195 (2019) highlighted the importance of the effective reaction probability (i.e., gamma number) of
196 heterogenous reaction between ozone and primary organic matter (POM) in simulating
197 stratospheric fire smoke lifetime.

198 The heterogeneous reaction of ozone and POM is not included in the standard EAMv1
199 release. In this study, the rate of the heterogeneous reaction (molecules cm^{-3} s^{-1}) is given by the
200 following:

201 $$R = \frac{1}{4}\gamma \nu_A A_p n_A, \quad (1)$$

202 where γ is the probability of the reaction, which is a perturbed parameter in the ensemble; ν_A is the
203 mean speed of ozone (cm s^{-1}); A_p is the total surface area of POM per unit volume of air (cm^2 cm^{-3});
204 n_A is the gas-phase concentration of ozone (molecules cm^{-3}) (Seinfeld & Pandis, 2012). We
205 assume that the ozone mixing ratio in the stratosphere will not be affected after the reaction, but
206 the POM concentration will decrease based on the reaction rate (Yu et al., 2019).

207 Running an ensemble of simulations with different parameter values can help determine
208 the parameter setting for minimizing differences between simulations and observations. Our
209 approach is to use an ensemble with four varied, or perturbed, parameters to determine the

parameter values which, when used in an E3SM simulation, produce the best fit to observations and equally importantly to quantify the model sensitivities to these parameters. We additionally use our ensemble to examine uncertainty within the E3SM simulations (Anderson & Lucas, 2018; Murphy et al., 2004), and would like to highlight that such an ensemble perturbation experiment has not been done for the 2017 pyroCb study before.

In this study, we run 144 simulations with varied values listed in Table 1. We add smoke at a variable injection height near 52°N, 120°W, where the 2017 pyroCb event was observed from the satellite remote sensing. The perturbed smoke amount and BC ratio is injected on a continuous basis for 5 hours from 19 UTC to 23 UTC on August 12, 2017. The injected smoke aerosols only contain BC and POM, which are added to the primary-carbon mode in MAM4. In addition to injecting an aerosol mass of BC and POM, the number concentration is also calculated based on the volume mean diameter (0.134 μm) and the BC/POM density (1.8/1.4 g cm^{-3}) (Liu et al., 2012).

Each ensemble member is given a name based on the value of four parameters. For example, 0.2Tg_BC2_12km_gamma6 means the simulation with 0.2 Tg smoke, of which 2% is BC, a 12 km smoke injection height, and a gamma number of 10^{-6} in the heterogeneous reaction calculation. We also run a control simulation (CNTL) without a smoke injection or a heterogeneous reaction applied to the POM.

2.4 Observations and the "ensemble score"

The Stratospheric Aerosol and Gas Experiment III (SAGE-III) is mounted on the International Space Station (ISS). SAGE-III Version 5.1 data from the instrument are available from June 2017, and level 2 data are used in this study. SAGE-III uses solar and lunar occultation and limb scatter to infer profiles of trace gases like ozone and aerosol extinction coefficient at nine wavelengths between 384 and 1544 nm. We choose to use the aerosol extinction coefficient at

1024 nm for most analyses in this study, which also follows the analysis in Yu et al. (2019). SAGE-III provides a nearly direct extinction measurement in its occultation mode, but the occultation measurement provides generally poor spatial coverage. The measurements only occur during the orbital sunrise and sunset. Thus, SAGE-III acquires 30 sets of profiles per day in two latitudes bands that roughly span 60°N to 60°S over a month. Details of SAGE-III ISS measurements are documented in Cisewski et al. (2014).

We use the SAGE-III aerosol extinction coefficient to derive daily aerosol optical depth (AOD) intergraded from 16 km to 20 km as the reference. Then, we compute daily AOD for each ensemble member to calculate the correlation and the mean square error (MSE) between modeled AOD and satellite retrieved AOD. Based on the correlation and MSE among all ensemble members, we can get an "ensemble score" for each member, which is defined as follows:

$$ensemble\ score = -normalized(MSE) + normalized(correlation) \quad (2)$$

Normalized MSE and correlation will get a number range from 0 to 1. A perfect ensemble case gets 1 as the highest ensemble score, which means MSE is zero and correlation gets 1 between modeled AOD and satellite retrieved AOD. Based on the ensemble scores, we can evaluate the model performance of an individual simulation, each with a unique combination of ensemble parameters.

2.5 Machine learning technique – Random Forest

Machine learning is now being used to quantify the performance of multi-model climate ensemble members (Monteleoni et al., 2011), determine the sensitivity of climate models to parameter values and resolution (Anderson & Lucas, 2018), and detect features in large climate data sets (Y. Liu et al., 2016). In this study, we apply a supervised machine learning technique, known as random forest (Breiman, 2001) to a perturbed smoke injection parameter ensemble of

EAMv1 simulations. We use the *feature importance* function in the scikit-learn random forest package (Pedregosa et al., 2011) to measure the importance of each feature. The function takes an array of features and computes the normalized total reduction of the criterion brought by that feature. In other words, features with high scores strongly partition the data and lie near the parent node in a decision tree. By perturbing the values of features in a tree and monitoring the fits' accuracy, each feature's importance is estimated. The highest score is the most important feature in the forecasting machine.

A group of randomized decision trees on different bootstrap samples of the training data is important to add a further level of randomness to splitting the trees. The scikit-learn random forest package we use in the study provides 50 trees, an internal bootstrap option, including the calculation of validation scores, and default settings for other fitting parameters. Furthermore, we also test the use of 10 or 100 decision trees for the training data to increase the variation of random forests. The train/test split varies from 70%/30% to 90%/10% with a 5% interval.

3 Results and discussions

3.1 Model evaluation of meteorological nudging

The relaxation time scale of nudging applied in global climate models is 6 hours in many previous studies, basically focusing on the tropospheric studies (Kooperman et al., 2012; Sun et al., 2019; Telford et al., 2008), but we find out this setup can strongly disturb the background aerosols in the stratosphere. Thus, we want to see how different nudging time scales affect EAMv1 results and, to the best of our knowledge, no EAMv1 papers have documented it. In a set of sensitivity tests of nudging U, V and T with different relaxation time scales, ranging from 6 to 50 hours, we find that while a shorter relaxation time scale can better constrain the meteorological

fields toward the ERA-Interim reanalysis data, the differences within this range are minor (figures not shown). However, a more significant issue, seldom mentioned in most studies, is that the background aerosol in the stratosphere becomes unrealistically high and deviates significantly from the control simulation without nudging.

Figure 1a shows the time series of area-averaged smoke mass mixing ratio (kg Tg-air^{-1}) in CNTL without meteorological nudging applied. The smoke aerosol mixing ratio above 15 km height is less than 0.1 kg Tg-air^{-1}, and the aerosol mixing ratio in the stratosphere should not be disturbed much by surface emissions, especially in the absence of extreme wildfire events or volcanic eruptions. However, once we apply the meteorological nudging with a 6-hour relaxation time scale, tropospheric aerosols are transported upward to the stratosphere, and accumulate with time due to the lack of wet scavenging at high altitudes (Figure 1b). Davis et al. (2022) suggested that a 12- to 24-hour nudging time scale is appropriate for minimizing errors, however, in our case, even with a relaxation time scale of 24 hours, the issue is not solved (Figure 1c). They also tried a 48-hour nudging time scale to eliminate the errors in the background and spatial patterns of constituents but at the cost of losing fidelity in the nudged variables. Because the purpose of nudging in this study is only to constrain synoptic variability, we use a 50-hour relaxation time scale to get stable stratospheric background aerosols (Figure 1d) without sacrificing too much accuracy of the nudged meteorological fields.

3.2 Ensemble runs and sensitivity to perturbed parameters

Examining the ensemble score (Eq. 2) for every ensemble member, we find the highest score is 0.96, achieved with the parameters set to 0.2 Tg of smoke, of which 2% is BC, with an injection height of 13.5 km, and a gamma value of 10^{-6} (named 0.2Tg_BC2_13.5km_gamma6). Time series of daily AOD integrated from 16 to 20 km in altitude is shown in Figure 2 from August

13, 2017, to May 31, 2018. This ensemble member captures the timing and value of AOD reasonably, as compared to the SAGE-III observations. The peak AOD from SAGE-III occurs in early September at about 0.002. The ensemble member 0.2Tg_BC2_13.5km_gamma6 roughly captures the timing of the peak in the AOD, but with a slightly higher value for a longer period of time, which continues into late September. After September, the AOD value and decay rate in 0.2Tg_BC2_13.5km_gamma6 compare well with the satellite retrieved AOD from SAGE-III.

In order to illustrate how sensitive the model is to each perturbed parameter, Figure 3 shows the boxplot of daily AOD of the member with the highest ensemble score (i.e., 0.2Tg_BC2_13.5km_gamma6) compared with the other ensemble members when each parameter is independently varied. Due to the overestimated modeled AOD in late September, the upper quartile and median of simulated AOD in 0.2Tg_BC2_13.5km_gamma6 are higher than the satellite retrieved AOD and the AOD of the other ensemble members for that month. Because AOD is derived directly from the smoke amount, the distinguishable AOD differences among the ensemble members with various smoke amounts are clearly shown in Figure 3a. On the other hand, the AOD in the other three perturbed parameter comparisons are more challenging to differentiate (Figures 3b – 3d). Figure 3 shows a common approach for the model intercomparison, but it could mislead one to conclude the model is most sensitive to smoke amount.

Figure 4 shows the boxplot and the mean ensemble score for four perturbed parameters. The mean ensemble score, for example, increases with smoke amount from 0.28 in the group of 0.2 Tg to 0.39 in the group of 0.4 Tg (Figure 4a). The mean ensemble score for simulations with varied BC ratio shows a similar trend, increasing with increased BC ratio, from 0.22 in the 1% BC group to 0.47 in the 5% BC group. Interestingly, when the injection height is varied, the highest mean ensemble score is 0.54 and occurs in the group with a 13 km injection height; while the

lowest mean score is 0.13 in the group with a 12 km injection height. This shows that the mean ensemble score changes significantly with different smoke injection heights. In other words, the model is more sensitive to the change of smoke injection height than to the other perturbed parameters. On the other hand, the mean ensemble score of the cases with a gamma number of 10^{-5}, 10^{-6}, and 10^{-7} are 0.36, 0.35, and 0.31, respectively. The ensemble score is similar across variation in the gamma number, meaning that the model shows little sensitivity to the choice of gamma number.

The *feature importance* function in the scikit-learn random forest package also calculates that injection height is the most important feature in this study with a score of 0.33, followed by BC ratio (0.28), smoke amount (0.22), and gamma number (0.16) (Figure 5). This result is consistent with what we show in Figure 4 – the larger variance of the mean ensemble scores, the more important feature is in the model.

3.3 Smoke transport and altitude

The 2017 pyroCb event was observed by the Cloud-Aerosol Lidar and Infrared Pathfinder Satellite Observation (CALIPSO) satellite, and the plume height was about 13.5 km on August 14 (Figure 5 in Das et al., 2021). At this altitude, the smoke is above the tropopause, and westerlies dominate the smoke transport. In our simulation, the smoke is transported to the East coast of the U.S. about 4 to 5 days after the fire smoke is injected (Figure 6b), and within 10 days, the smoke reaches most European countries (Figure 6d).

We notice that as the smoke aerosols approach Hudson Bay in eastern Canada, the smoke is transported southward due to the jet stream (Figure 6b). Once the smoke moves to the lower midlatitudes (~45°N) and rises to a height of ~18 km, the dominant winds change from westerlies to easterlies, so the smoke transport turns westward (Figure 6c-e). Therefore, this pyroCb event

has two transport paths in the stratosphere, and the smoke aerosols rapidly spread over the entire midlatitude area within three weeks after the smoke is injected (Figure 6e). In late September 2017, the fire smoke aerosols cover almost the entire northern hemisphere (Figure 6f).

Our result shows that plume rise height is important to the plume transport and smoke aerosol concentration in the lower stratosphere. Based on the definition of maximum plume height in Thomason et al. (2018), where the aerosol extinction coefficient is greater than 1.5×10^{-4} km^{-1}, 50% higher than the background value in the lower stratosphere, our simulated maximum plume rise height in 0.2Tg_BC2_13.5km_gamma6 matches the plume rise height observed by SAGE-III well (Figure 7). The initial rise of the modeled plume occurs at a rate of 0.25 km day^{-1}, attaining heights of 20 km in late September. It is noted here that once the smoke aerosol is injected into the stratosphere, the plume rise does not rely only on vertical motions within the atmosphere, but also on heating of the black carbon through absorption of shortwave solar radiation (Yu et al., 2019). Heating of the black carbon is considered in EAMv1, but the internal mixing state of aerosols in MAM4 does not perfectly represent the core-shell structure of BC with other chemical species.

3.4 Smoke lifetime and radiative effects

As discussed earlier, Wagman et al. (2020) used an older EAMv1 configuration to examine the climate impacts of mass urban fires in South Asia induced by a regional nuclear exchange scenario. Their study showed a shorter smoke lifetime in the stratosphere than in other similar studies, which is one motivation for the work here. In this work, our calculation for the 2017 pyroCb smoke lifetime in the stratosphere reasonably matches the observations and previous studies. Figure 8a shows the decay rate of EAMv1 aerosol optical depth (blue dashed line), which is calculated starting from September 1, 2017. Based on this decay rate, the model gives an e-

370 folding time of 178 days, while on the same starting day, an e-folding time of 227 days is calculated
371 from SAGE-III data. The estimated e-folding time only changes by one or two days in either
372 EAMv1 or SAGE-III when the decay period starts from mid-September, which is the peak of
373 AOD. This suggests little sensitivity to the start date.

374 Yu et al. (2019) reported that the lifetime of the stratospheric smoke was observed to be
375 ~150 days for the 2017 pyroCb events. We use another quantity, the smoke column mass
376 (BC+POM) concentration, to calculate an e-folding time of ~120 days, which is consistent with
377 observations from SAGE-III depicted in Yu et al. (2019) (Figure 8b). Das et al. (2021), also
378 reported an e-folding time of ~140-150 days from their results running the Goddard Earth
379 Observing System (GEOS) atmospheric general circulation model (AGCM) and the also from
380 OMPS-LP (Ozone Mapping Profiler Suite Limb Profiler) observations. Our study and Yu et al.
381 (2019) considered the heterogeneous reaction between organics present in the smoke and ozone in
382 the stratosphere, which plays a role in matching the observed decay. By contrast, in Das et al.
383 (2021) and Christian et al. (2019), this heterogeneous reaction is not considered, and the pyroCb
384 smoke lifetime is simply the dynamical lifetime of the smoke in the model, which includes the
385 removal by large scale circulations, aerosol sedimentation, and aerosol radiative heating/cooling.

386 Due to the long lifetime and wide transport of stratospheric aerosols, the pyroCb injected
387 stratospheric smoke can affect the global radiative budget. Figure 9a shows the spatial-temporal
388 averaged radiative effects of simulated smoke aerosols over the northern hemisphere from August
389 13, 2017, to May 31, 2018. The main impact of the stratospheric smoke aerosols is shortwave
390 surface cooling, which has an averaged value of -0.334 W m^{-2}. The absorption of solar radiation
391 also causes warming in the atmosphere by 0.257 W m^{-2}. Since the longwave radiative effects of

stratospheric aerosols are minor, the net radiative effects of smoke aerosols are close to the shortwave values (Figure 9a).

The radiative effects of smoke aerosols are small in the long-term average. However, the pyroCb aerosols have strong atmospheric warming and surface cooling effects for about 2-3 months after the smoke injections (Figure 9b and 9c). The atmospheric warming and surface cooling are most pronounced between 30 - 80°N, consistent with Das et al. (2021). The maximum values of the net radiative effect occurs within the first 7-10 days after the smoke injections, causing atmospheric warming up to 3.84 W m^{-2} and a surface cooling of about -5.10 W m^{-2}. Our calculated radiative effects in Figure 9b and 9c are similar to the results presented in Das et al. (2021), which found that the pyroCb smoke particles result in a maximum radiative warming of 8.3 W m^{-2} in the atmosphere and radiative cooling of -5.4 W m^{-2} at the surface. It is noted that their results are all-sky radiative effects, but Figure 9 are clear-sky radiative effects.

4 Discussion

Figure 2 shows that our simulated AOD from the best ensemble case, 0.2Tg_BC2_13km_gamma6, matches the derived AOD from SAGE-III well. However, we notice that the modeled extinctions are overestimated in the lower stratosphere, in comparison to the observations (Figure 10a). The modeled smoke extinctions are much higher than the extinctions from SAGE-III at the beginning of the injection. Once the modeled extinctions reach the peak at 16 km height, the rate of the modeled smoke extinction declines slower than the observed rate. By contrast, the model underestimates the extinction coefficient at the altitude of 20 km (Figure 10c). The modeled extinctions match the observed extinctions well in the first few weeks after the injection, even background stratospheric aerosol extinction at the beginning of the pyroCb events.

However, the descending rate of the modeled extinction is faster than the observed extinction, especially at a height of 20 km.

In Das et al. (2021), the modeled result also has a negative bias at higher altitudes (> 20 km) and a positive bias at lower altitudes, especially for the first 10-20 days after the smoke injection. Based on their explanation, there are two reasons - the modeled background stratospheric aerosol extinctions are lower than OMPS-LP retrievals at the higher levels (a negative bias at higher altitudes), and the modeled smoke plumes are lower than the observed plumes, which reached as high as 22 km (a positive bias at lower altitudes). In our simulation, the modeled background aerosol extinctions are comparable with SAGE-III. The main reason for the biases of modeled extinctions could be a combination of errors in the smoke self-lofting and coarse vertical resolution at these altitudes.

As we mentioned in Section 3.3, the self-lofting of smoke aerosols comes from heating of the black carbon, which is included in EAMv1, but the internal mixing state of aerosols in MAM4 does not perfectly represent the core-shell structure of BC with other chemical species. The mixing state of aerosols affects aerosol growth and radiative forcing. Thus, the model is not sensitive to changes in the BC ratio and does not generate strong vertical motions from the heating of the black carbon. The other possible reason is the coarse vertical resolution. EAMv1 has a traditional hybridized sigma pressure vertical coordinate. The vertical resolution in the stratosphere in EAMv1 is about 450 – 800 m, which is much coarser than the resolution in the lower troposphere (dz = ~100 m). Regardless of if the vertical motion of the smoke aerosols is caused by dynamics or thermal buoyancy, the coarse vertical resolution cannot represent the vertical transport properly. The coarse vertical resolution could be one reason why, although the smoke aerosols are injected

436 at the correct height, aerosols descend at different rates in the lower and higher stratosphere (Figure
437 10).

438 5 Summary

439 We use EAMv1 to reexamine the 2017 pyroCb events over British Columbia and complete
440 an ensemble of runs targeting three uncertain injection parameters: smoke amount, the ratio of
441 black carbon to the smoke amount, and injection height. We also consider the probability
442 parameter of the heterogeneous reaction of ozone and organic carbon suggested by Yu et al.
443 (2019). According to the daily aerosol optical depth (AOD) integrated from 16 km to 20 km,
444 derived from the SAGE-III aerosol extinction coefficient at 1024 nm wavelength, we define an
445 "ensemble score" for each member and get a highest score of 0.96 achieved by the ensemble
446 member 0.2Tg_BC2_13.5km_gamma6,which has 0.2 Tg of smoke , 2% of which is BC, a 13.5
447 km smoke injection height, and 10^{-6} gamma number in the heterogeneous reaction.

448 The case of 0.2Tg_BC2_13.5km_gamma6 captures the time of the peak in AOD and also
449 the decay rate, as compared to the satellite retrieved AOD from SAGE-III. We examine model
450 sensitivity to different values of each perturbed parameter (i.e., smoke amount, the ratio of black
451 carbon to smoke, injection height, and gamma number), and the results show that the model is
452 more sensitive to a change in smoke injection height and less sensitive to variation in the gamma
453 number. This conclusion is supported by the *feature importance* function in the scikit-learn
454 random forest package. The injection height is the most important feature in this study, with a
455 score of 0.33, followed by BC ratio (0.28), smoke amount (0.22), and gamma number (0.16).

456 The pyroCb smoke aerosols simulated in this study have two main transport paths in the
457 stratosphere. The smoke aerosols rapidly spread throughout the entire midlatitude area within
458 three weeks after the smoke is injected and cover almost the entire northern hemisphere for about

50 days. Our calculation for the 2017 pyroCb smoke lifetime in the stratosphere reasonably matches the observations and previous studies. Based on the decay rate of daily AOD, the model gives an e-folding time of 178 days, while SAGE-III suggests an e-folding time of 227 days. We use another quantity, the smoke column mass (BC+POM) concentration, to calculate an e-folding time at different level heights, and our estimated e-folding time is consistent with observations from SAGE-III, about 120 days.

Due to the long lifetime and wide transport of stratospheric aerosols, the radiative effects of the pyroCb injected smoke in the stratosphere can be important in the global radiation budget. The pyroCb aerosols have strong atmospheric warming and surface cooling effects for about 2-3 months after the smoke injection. The atmospheric warming and surface cooling are most pronounced between 30 - 80°N. Averaging the entire simulation period, the major impact of stratospheric aerosols is the shortwave surface cooling, which has a spatiotemporal averaged value of -0.334 W m^{-2} over the north hemisphere from August 13, 2017, to May 31, 2018. The shortwave radiative effects of stratospheric aerosols also cause warming in the atmosphere by 0.257 W m^{-2}.

Our simulated AOD from the best ensemble member, 0.2Tg_BC2_13km_gamma6, matches the derived AOD from SAGE-III well. However, the modeled aerosol extinctions have a negative bias at the higher altitudes (~ 20 km) and a positive bias lower in the stratosphere (~16 km). The combination of the internal mixing state of aerosols in MAM4 and the coarse vertical resolution in the stratosphere could cause the model to lack fidelity in simulating smoke aerosol self-lofting and vertical motions. Thus, further studies are needed to get a realistic aerosol mixing structure in MAM4 and a higher vertical resolution in the stratosphere.

Code and data availability:

The model code used in this study is located at https://doi.org/10.5281/zenodo.6383271. The extinction coefficient simulated by EAMv1 can be found at https://doi.org/10.5281/zenodo.6383299. Other EAMv1 simulated outputs are available upon request from Hsiang-He Lee (lee1061@llnl.gov).

Acknowledgements:

This work is partially supported by the Department of Energy National Nuclear Security Administration Office of Nonproliferation and Arms Control. Support has also been received from the Lawrence Livermore National Laboratory (LLNL) LDRD projects 22-ERD-008, "Multiscale Wildfire Simulation Framework and Remote Sensing" and 18-ERD-049, "Modeling Nuclear Cloud Rise and Fallout in Complex Environments". Work at LLNL was performed under the auspices of the U.S. DOE by Lawrence Livermore National Laboratory under contract DE-AC52-07NA27344. LLNL IM: LLNL-JRNL-833029-DRAFT.

Reference

Anderson, G. J., & Lucas, D. D. (2018). Machine Learning Predictions of a Multiresolution Climate Model Ensemble. *Geophysical Research Letters, 45*(9), 4273-4280. doi:https://doi.org/10.1029/2018GL077049

Andreae, M. O. (2019). Emission of trace gases and aerosols from biomass burning – an updated assessment. *Atmos. Chem. Phys., 19*(13), 8523-8546. doi:10.5194/acp-19-8523-2019

Andreae, M. O., & Merlet, P. (2001). Emission of trace gases and aerosols from biomass burning. *Global Biogeochemical Cycles, 15*(4), 955-966. doi:https://doi.org/10.1029/2000GB001382

Bergstrom, R. W., Russell, P. B., & Hignett, P. (2002). Wavelength Dependence of the Absorption of Black Carbon Particles: Predictions and Results from the TARFOX Experiment and Implications for the Aerosol Single Scattering Albedo. *Journal of the Atmospheric Sciences, 59*(3), 567-577. doi:10.1175/1520-0469(2002)059<0567:Wdotao>2.0.Co;2

Breiman, L. (2001). Random forests. *Machine learning, 45*(1), 5-32.

Christian, K., Wang, J., Ge, C., Peterson, D., Hyer, E., Yorks, J., & McGill, M. (2019). Radiative Forcing and Stratospheric Warming of Pyrocumulonimbus Smoke Aerosols: First Modeling Results With Multisensor (EPIC, CALIPSO, and CATS) Views from Space. *Geophysical Research Letters, 46*(16), 10061-10071. doi:https://doi.org/10.1029/2019GL082360

Cisewski, M., Zawodny, J., Gasbarre, J., Eckman, R., Topiwala, N., Rodriguez-Alvarez, O., . . . Hall, S. (2014). *The Stratospheric Aerosol and Gas Experiment (SAGE III) on the International Space Station (ISS) Mission* (Vol. 9241): SPIE.

Das, S., Colarco, P. R., Oman, L. D., Taha, G., & Torres, O. (2021). The long-term transport and radiative impacts of the 2017 British Columbia pyrocumulonimbus smoke aerosols in the stratosphere. *Atmos. Chem. Phys., 21*(15), 12069-12090. doi:10.5194/acp-21-12069-2021

Davis, N. A., Callaghan, P., Simpson, I. R., & Tilmes, S. (2022). Specified dynamics scheme impacts on wave-mean flow dynamics, convection, and tracer transport in CESM2 (WACCM6). *Atmos. Chem. Phys., 22*(1), 197-214. doi:10.5194/acp-22-197-2022

ERA-Interim Project. (2009). Retrieved from: https://doi.org/10.5065/D6CR5RD9

Fromm, M., Alfred, J., Hoppel, K., Hornstein, J., Bevilacqua, R., Shettle, E., . . . Stocks, B. (2000). Observations of boreal forest fire smoke in the stratosphere by POAM III, SAGE II, and lidar in 1998. *Geophysical Research Letters, 27*(9), 1407-1410. doi:https://doi.org/10.1029/1999GL011200

Fromm, M., Bevilacqua, R., Servranckx, R., Rosen, J., Thayer, J. P., Herman, J., & Larko, D. (2005). Pyro-cumulonimbus injection of smoke to the stratosphere: Observations and impact of a super blowup in northwestern Canada on 3–4 August 1998. *Journal of Geophysical Research: Atmospheres, 110*(D8). doi:https://doi.org/10.1029/2004JD005350

Fromm, M., Lindsey, D. T., Servranckx, R., Yue, G., Trickl, T., Sica, R., . . . Godin-Beekmann, S. (2010). The Untold Story of Pyrocumulonimbus. *Bulletin of the American Meteorological Society, 91*(9), 1193-1210. doi:10.1175/2010bams3004.1

Ge, C., Wang, J., Carn, S., Yang, K., Ginoux, P., & Krotkov, N. (2016). Satellite-based global volcanic SO2 emissions and sulfate direct radiative forcing during 2005–2012. *Journal of Geophysical Research: Atmospheres, 121*(7), 3446-3464. doi:https://doi.org/10.1002/2015JD023134

Golaz, J.-C., Caldwell, P. M., Van Roekel, L. P., Petersen, M. R., Tang, Q., Wolfe, J. D., . . . Zhu, Q. (2019). The DOE E3SM Coupled Model Version 1: Overview and Evaluation at Standard Resolution. *Journal of Advances in Modeling Earth Systems, 11*(7), 2089-2129. doi:10.1029/2018ms001603

Hofmann, D., Barnes, J., O'Neill, M., Trudeau, M., & Neely, R. (2009). Increase in background stratospheric aerosol observed with lidar at Mauna Loa Observatory and Boulder, Colorado. *Geophysical Research Letters, 36*(15). doi:https://doi.org/10.1029/2009GL039008

Hsu, J., & Prather, M. J. (2009). Stratospheric variability and tropospheric ozone. *Journal of Geophysical Research: Atmospheres, 114*(D6). doi:https://doi.org/10.1029/2008JD010942

Kooperman, G. J., Pritchard, M. S., Ghan, S. J., Wang, M., Somerville, R. C. J., & Russell, L. M. (2012). Constraining the influence of natural variability to improve estimates of global aerosol indirect effects in a nudged version of the Community Atmosphere Model 5. *Journal of Geophysical Research: Atmospheres, 117*(D23). doi:https://doi.org/10.1029/2012JD018588

555 Liu, X., Easter, R. C., Ghan, S. J., Zaveri, R., Rasch, P., Shi, X., . . . Mitchell, D. (2012). Toward
556 a minimal representation of aerosols in climate models: description and evaluation in the
557 Community Atmosphere Model CAM5. *Geosci. Model Dev., 5*(3), 709-739.
558 doi:10.5194/gmd-5-709-2012
559 Liu, X., Ma, P. L., Wang, H., Tilmes, S., Singh, B., Easter, R. C., . . . Rasch, P. J. (2016).
560 Description and evaluation of a new four-mode version of the Modal Aerosol Module
561 (MAM4) within version 5.3 of the Community Atmosphere Model. *Geosci. Model Dev.,*
562 *9*(2), 505-522. doi:10.5194/gmd-9-505-2016
563 Liu, Y., Racah, E., Correa, J., Khosrowshahi, A., Lavers, D., Kunkel, K., . . . Collins, W. (2016).
564 Application of deep convolutional neural networks for detecting extreme weather in
565 climate datasets. *arXiv preprint arXiv:1605.01156*.
566 Malone, R. C., Auer, L. H., Glatzmaier, G. A., Wood, M. C., & Toon, O. B. (1985). Influence of
567 Solar Heating and Precipitation Scavenging on the Simulated Lifetime of
568 Post—Nuclear War Smoke. *Science, 230*(4723), 317-319.
569 doi:doi:10.1126/science.230.4723.317
570 Mills, M. J., Toon, O. B., Lee-Taylor, J., & Robock, A. (2014). Multidecadal global cooling and
571 unprecedented ozone loss following a regional nuclear conflict. *Earth's Future, 2*(4), 161-
572 176. doi:https://doi.org/10.1002/2013EF000205
573 Monteleoni, C., Schmidt, G. A., Saroha, S., & Asplund, E. (2011). Tracking climate models.
574 *Statistical Analysis and Data Mining: The ASA Data Science Journal, 4*(4), 372-392.
575 doi:https://doi.org/10.1002/sam.10126
576 Murphy, J. M., Sexton, D. M. H., Barnett, D. N., Jones, G. S., Webb, M. J., Collins, M., &
577 Stainforth, D. A. (2004). Quantification of modelling uncertainties in a large ensemble of
578 climate change simulations. *Nature, 430*(7001), 768-772. doi:10.1038/nature02771
579 Park, R. J., Jacob, D. J., Chin, M., & Martin, R. V. (2003). Sources of carbonaceous aerosols over
580 the United States and implications for natural visibility. *Journal of Geophysical Research:*
581 *Atmospheres, 108*(D12). doi:https://doi.org/10.1029/2002JD003190
582 Pedregosa, F., Varoquaux, G., Gramfort, A., Michel, V., Thirion, B., Grisel, O., . . . Dubourg, V.
583 (2011). Scikit-learn: Machine learning in Python. *the Journal of machine Learning*
584 *research, 12*, 2825-2830.
585 Peterson, D. A., Campbell, J. R., Hyer, E. J., Fromm, M. D., Kablick, G. P., Cossuth, J. H., &
586 DeLand, M. T. (2018). Wildfire-driven thunderstorms cause a volcano-like stratospheric
587 injection of smoke. *npj Climate and Atmospheric Science, 1*(1), 30. doi:10.1038/s41612-
588 018-0039-3
589 Rasch, P. J., Xie, S., Ma, P.-L., Lin, W., Wang, H., Tang, Q., . . . Yang, Y. (2019). An Overview
590 of the Atmospheric Component of the Energy Exascale Earth System Model. *Journal of*
591 *Advances in Modeling Earth Systems, 11*(8), 2377-2411. doi:10.1029/2019ms001629
592 Reisner, J., D'Angelo, G., Koo, E., Even, W., Hecht, M., Hunke, E., . . . Cooley, J. (2018). Climate
593 Impact of a Regional Nuclear Weapons Exchange: An Improved Assessment Based On
594 Detailed Source Calculations. *Journal of Geophysical Research: Atmospheres, 123*(5),
595 2752-2772. doi:https://doi.org/10.1002/2017JD027331
596 Schwarz, J. P., Samset, B. H., Perring, A. E., Spackman, J. R., Gao, R. S., Stier, P., . . . Fahey, D.
597 W. (2013). Global-scale seasonally resolved black carbon vertical profiles over the Pacific.
598 *Geophysical Research Letters, 40*(20), 5542-5547.
599 doi:https://doi.org/10.1002/2013GL057775

Seinfeld, J. H., & Pandis, S. N. (2012). *Atmospheric chemistry and physics: from air pollution to climate change* (2 ed.): Wiley.

Sun, J., Zhang, K., Wan, H., Ma, P.-L., Tang, Q., & Zhang, S. (2019). Impact of Nudging Strategy on the Climate Representativeness and Hindcast Skill of Constrained EAMv1 Simulations. *Journal of Advances in Modeling Earth Systems, 11*(12), 3911-3933. doi:https://doi.org/10.1029/2019MS001831

Tang, Q., Klein, S. A., Xie, S., Lin, W., Golaz, J. C., Roesler, E. L., . . . Zheng, X. (2019). Regionally refined test bed in E3SM atmosphere model version 1 (EAMv1) and applications for high-resolution modeling. *Geosci. Model Dev., 12*(7), 2679-2706. doi:10.5194/gmd-12-2679-2019

Telford, P. J., Braesicke, P., Morgenstern, O., & Pyle, J. A. (2008). Technical Note: Description and assessment of a nudged version of the new dynamics Unified Model. *Atmos. Chem. Phys., 8*(6), 1701-1712. doi:10.5194/acp-8-1701-2008

Thomason, L. W., Ernest, N., Millán, L., Rieger, L., Bourassa, A., Vernier, J. P., . . . Peter, T. (2018). A global space-based stratospheric aerosol climatology: 1979–2016. *Earth Syst. Sci. Data, 10*(1), 469-492. doi:10.5194/essd-10-469-2018

Torres, O., Bhartia, P. K., Taha, G., Jethva, H., Das, S., Colarco, P., . . . Ahn, C. (2020). Stratospheric Injection of Massive Smoke Plume From Canadian Boreal Fires in 2017 as Seen by DSCOVR-EPIC, CALIOP, and OMPS-LP Observations. *Journal of Geophysical Research: Atmospheres, 125*(10), e2020JD032579. doi:https://doi.org/10.1029/2020JD032579

Vernier, J. P., Pommereau, J. P., Garnier, A., Pelon, J., Larsen, N., Nielsen, J., . . . McDermid, I. S. (2009). Tropical stratospheric aerosol layer from CALIPSO lidar observations. *Journal of Geophysical Research: Atmospheres, 114*(D4). doi:https://doi.org/10.1029/2009JD011946

Wagman, B. M., Lundquist, K. A., Tang, Q., Glascoe, L. G., & Bader, D. C. (2020). Examining the Climate Effects of a Regional Nuclear Weapons Exchange Using a Multiscale Atmospheric Modeling Approach. *Journal of Geophysical Research: Atmospheres, 125*(24), e2020JD033056. doi:https://doi.org/10.1029/2020JD033056

Wang, H., Easter, R. C., Zhang, R., Ma, P.-L., Singh, B., Zhang, K., . . . Yoon, J.-H. (2020). Aerosols in the E3SM Version 1: New Developments and Their Impacts on Radiative Forcing. *Journal of Advances in Modeling Earth Systems, 12*(1), e2019MS001851. doi:10.1029/2019ms001851

Wang, J., Park, S., Zeng, J., Ge, C., Yang, K., Carn, S., . . . Omar, A. H. (2013). Modeling of 2008 Kasatochi volcanic sulfate direct radiative forcing: assimilation of OMI SO₂ plume height data and comparison with MODIS and CALIOP observations. *Atmos. Chem. Phys., 13*(4), 1895-1912. doi:10.5194/acp-13-1895-2013

Yu, P., Toon, O. B., Bardeen, C. G., Zhu, Y., Rosenlof, K. H., Portmann, R. W., . . . Robock, A. (2019). Black carbon lofts wildfire smoke high into the stratosphere to form a persistent plume. *Science, 365*(6453), 587-590. doi:10.1126/science.aax1748

642 Table 1. The range of parameters describing the smoke injection and the gamma number of the
643 heterogenous reaction of ozone and particulate organic matter in the ensemble runs
644

Parameter (unit)	Range
Smoke amount (Tg)	[0.2, 0.3, 0.4]
BC to smoke ratio (%)	[1, 2, 3, 5]
Injection height (km)	[12, 12.5, 13, 13.5]
Gamma number (unitless)	[10^{-7}, 10^{-6}, 10^{-5}]

645
646

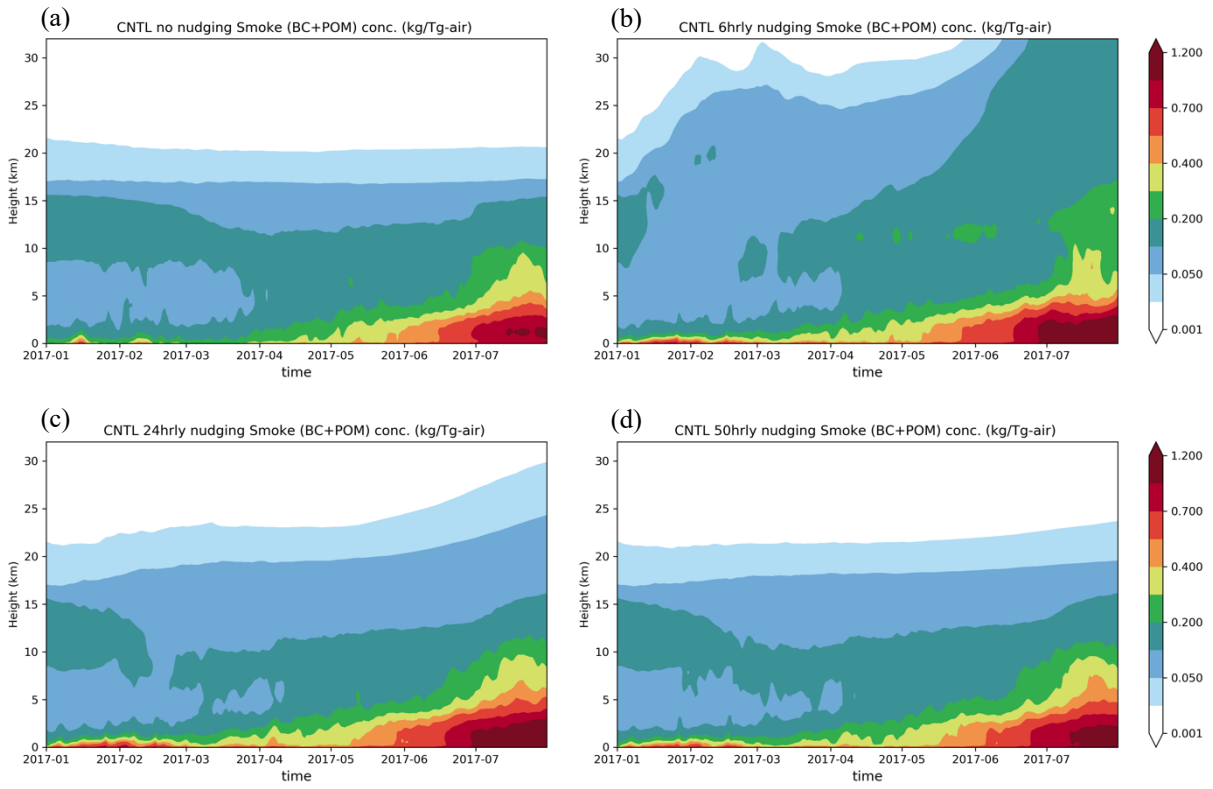

Figure 1. (a) Time series of area-averaged smoke (BC+POM) mass mixing ratio (kg Tg-air^{-1}) in the control simulation (CNTL) without meteorological nudging applied. (b) – (d) The same as in (a), but with the horizontal wind components and temperature nudged toward the ERA-Interim reanalysis data with 6, 24, and 50-hour relaxation time scales, respectively. Area is averaged from a latitude of 40°N to 80°N.

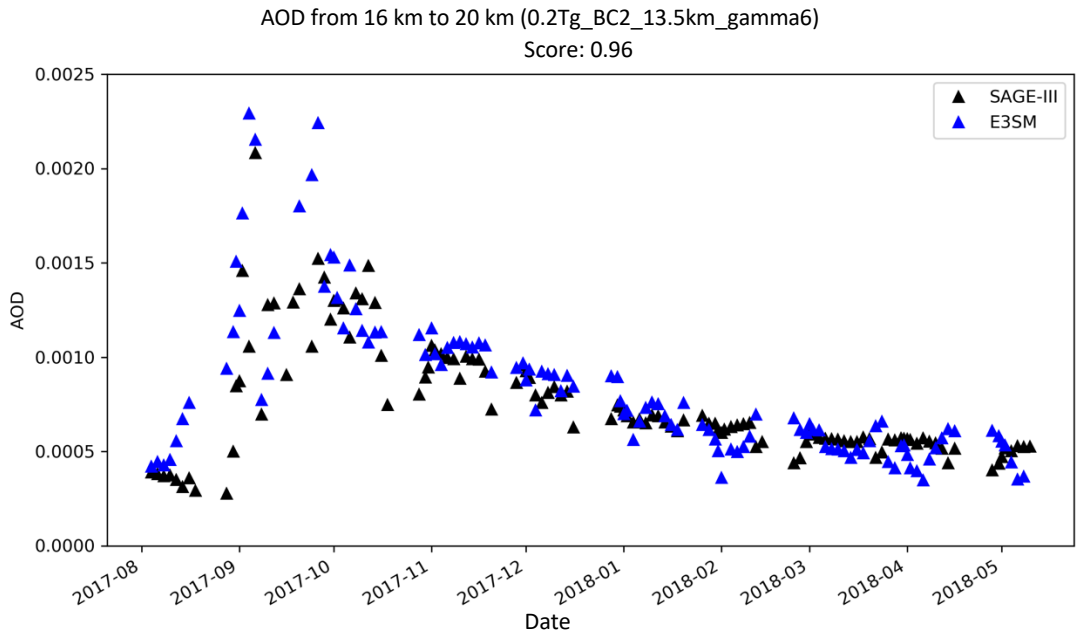

Figure 2. Time series of daily AOD (unitless) integrated from 16 km to 20 km in height. Black triangles are the derived AOD from SAGE-III, while blue triangles indicate the simulated AOD from the best performing ensemble member (0.2Tg_BC2_13.5km_gamma6). The ensemble score is calculated from Aguest 13, 2017 to May 31, 2018.

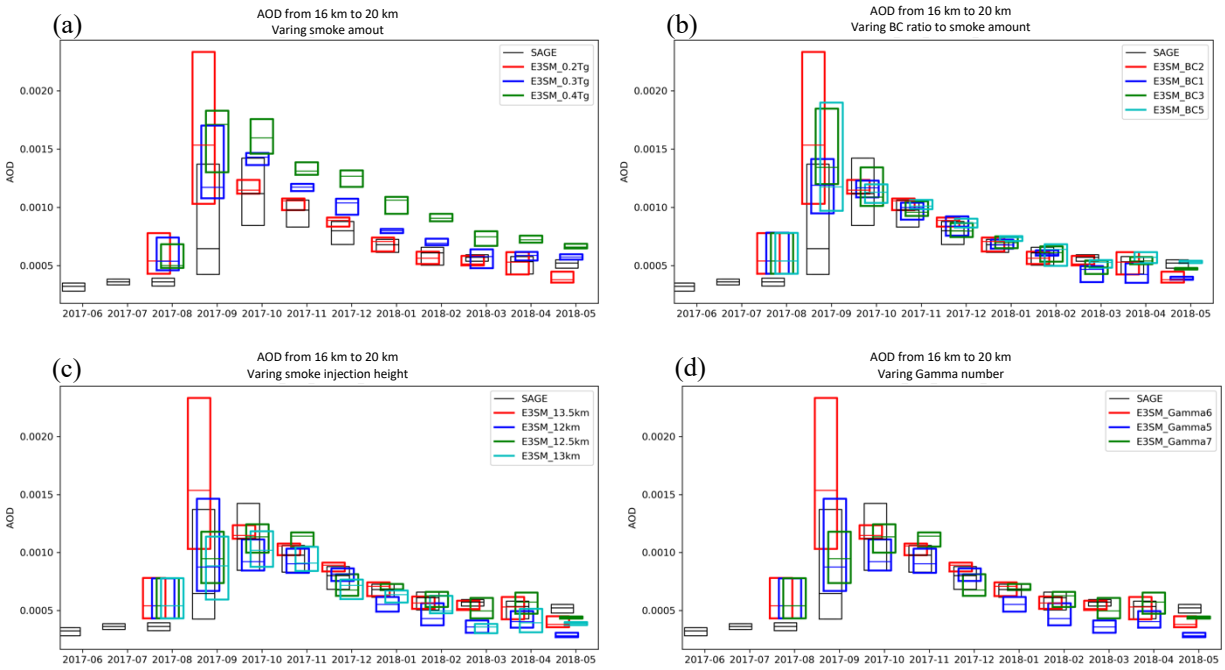

Figure 3. (a) Boxplot of daily AOD for the best performing ensemble member (0.2Tg_BC2_13.5km_gamma6; red boxes) along with other ensemble members with varied smoke amounts. (b) – (d) The same as (a) but varying BC ratio, injection height, and gamma number, respectively. The black boxes show the retrieved AOD from SAGE-III. The horizontal lines of the boxplot indicate the lower quartile, the median, and the upper quartile of daily AOD.

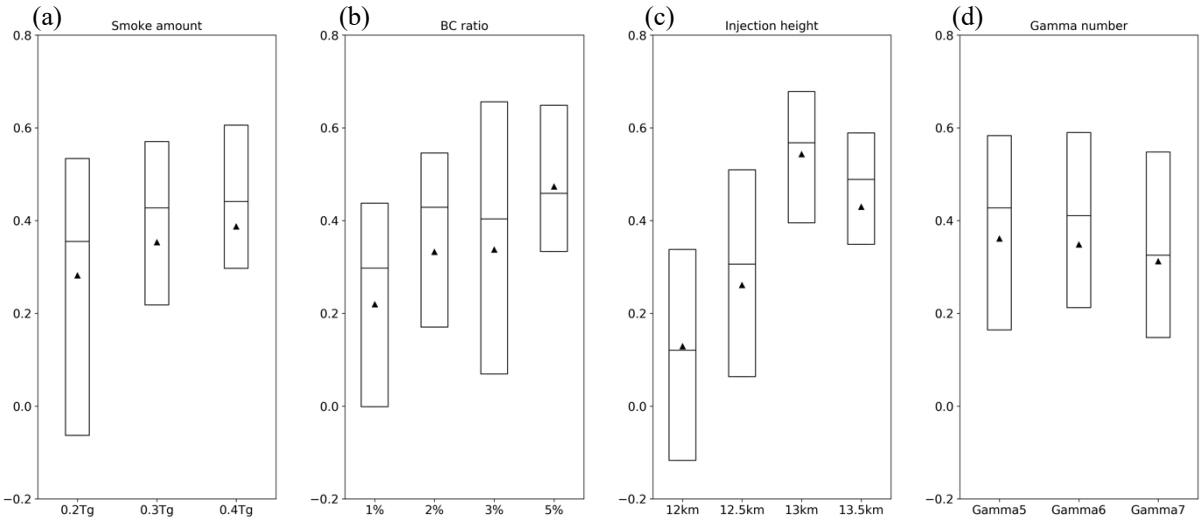

Figure 4. The boxplot and the mean of ensemble score for four perturbed parameters. The boxplot displays the lower quartile, the median, and the upper quartile of ensemble score for each variable number. The triangle is the mean of ensemble score for each variable number. Each ensemble score is calculated from August 13, 2017 to May 31, 2018.

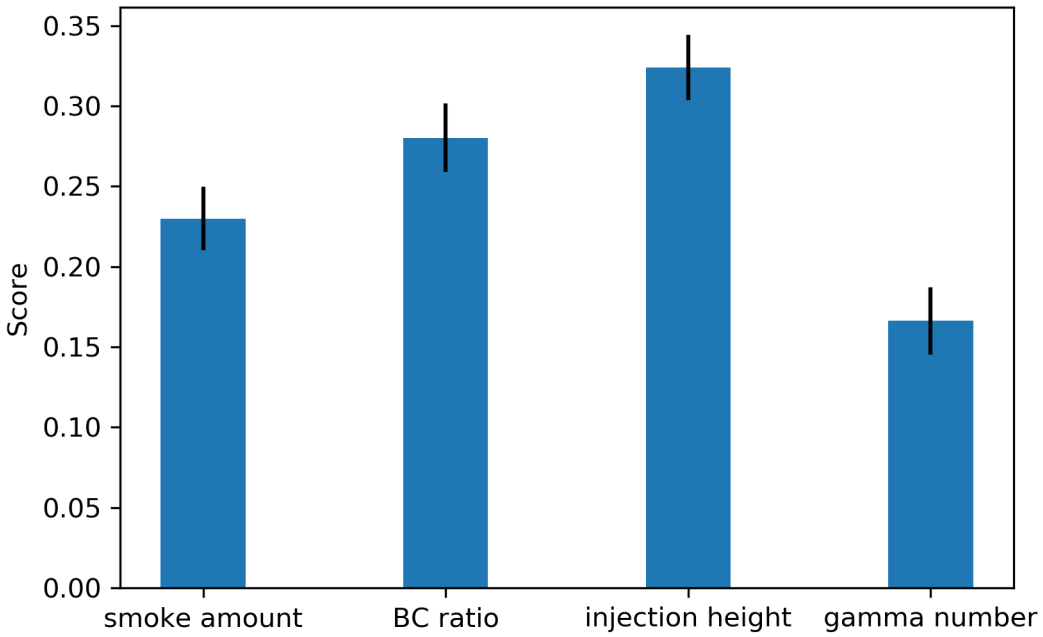

Figure 5. Feature importance calculated by the scikit-learn random forest package. Desired outputs are high ensemble scores. The feature inputs are listed in Table 1. The error bar is given by the 15 random forest runs with different splitting of trees and training samples. The detail of the model set up is presented in Section 2.5.

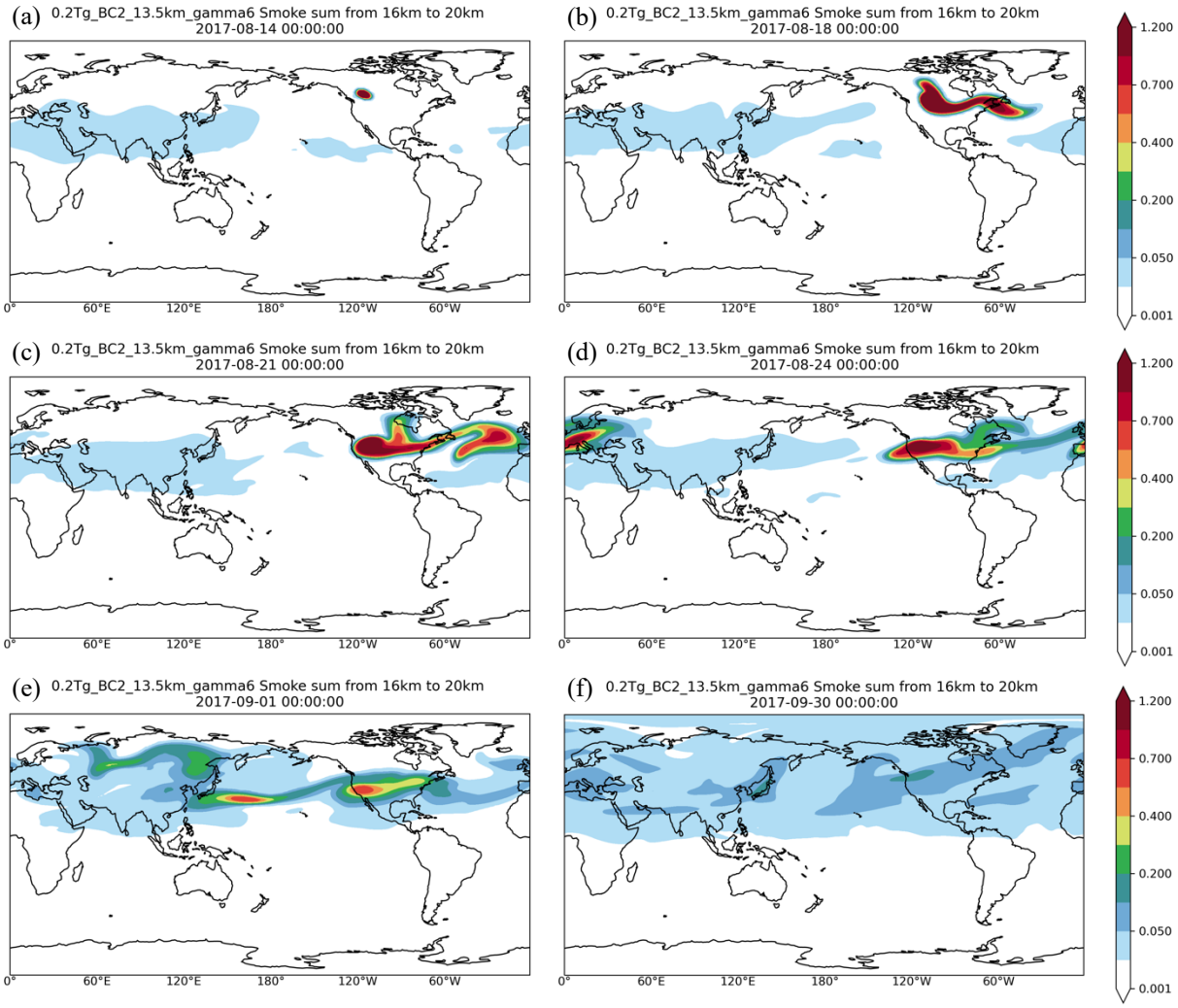

Figure 6. Integrated smoke concentration ($\times 10^{-7}$ kg m^{-2}) from 16 km to 20 km in altitude for the case of 0.2Tg_BC2_13.5km_gamma6. (a) – (f) are the smoke transport on August 14, August 18, August 21, August 28, September 1, and September 30, 2017, respectively.

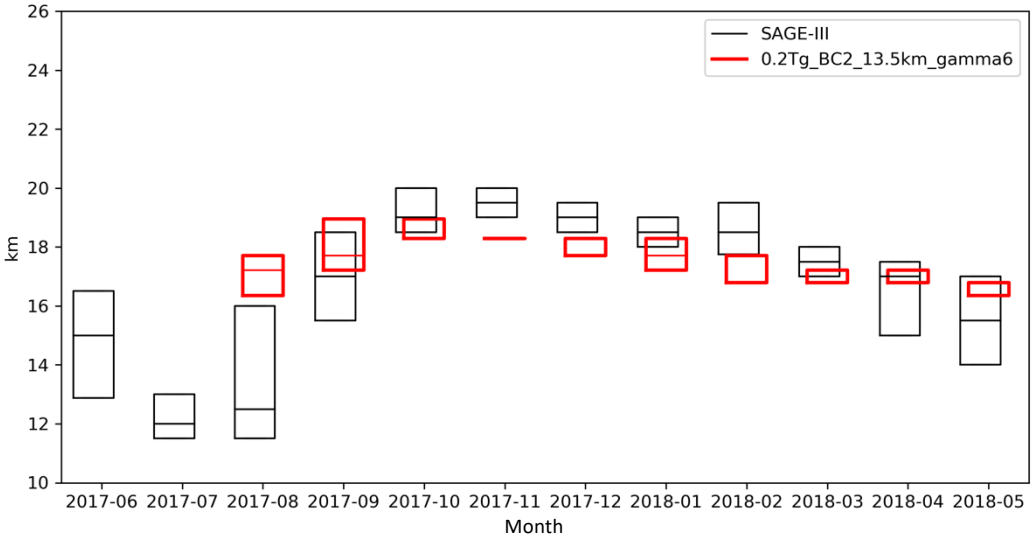

Figure 7. A boxplot of daily maximum plume height in 0.2Tg_BC2_13.5km_gamma6 (red boxes) compared with SAGE-III observations (black boxes). Plume height is defined as the height at which the aerosol extinction coefficient is greater than 1.5×10^{-4} km^{-1}. The boxplot displays the lower quartile, median, and upper quartile of the daily maximum plume height.

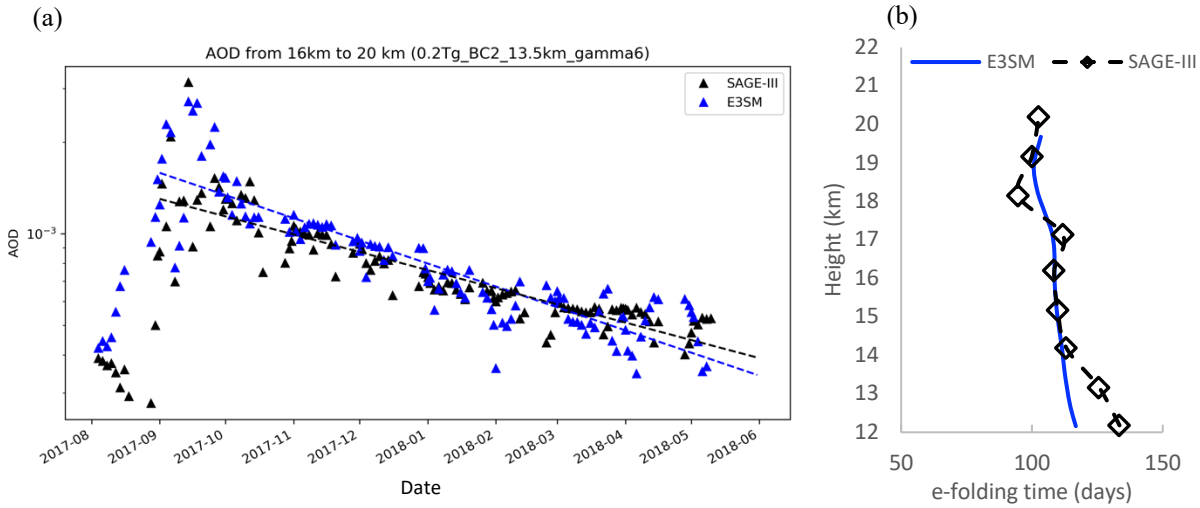

Figure 8. (a) Daily AOD as in Figure 2, but a logarithmic scale is used for the y-axis. The decay rate of E3SM AOD (blue dashed line) is calculated starting from September 1, 2017. (b) Altitude-dependent lifetime for the smoke column mass (BC+POM) concentration above each altitude in 0.2Tg_BC2_13.5km_gamma6 (blue line). Calculated smoke lifetime from SAGE-III data is the smoke column optical depth above each altitude shown by the dashed line with diamond symbols (as depicted in Yu et al. (2019)).

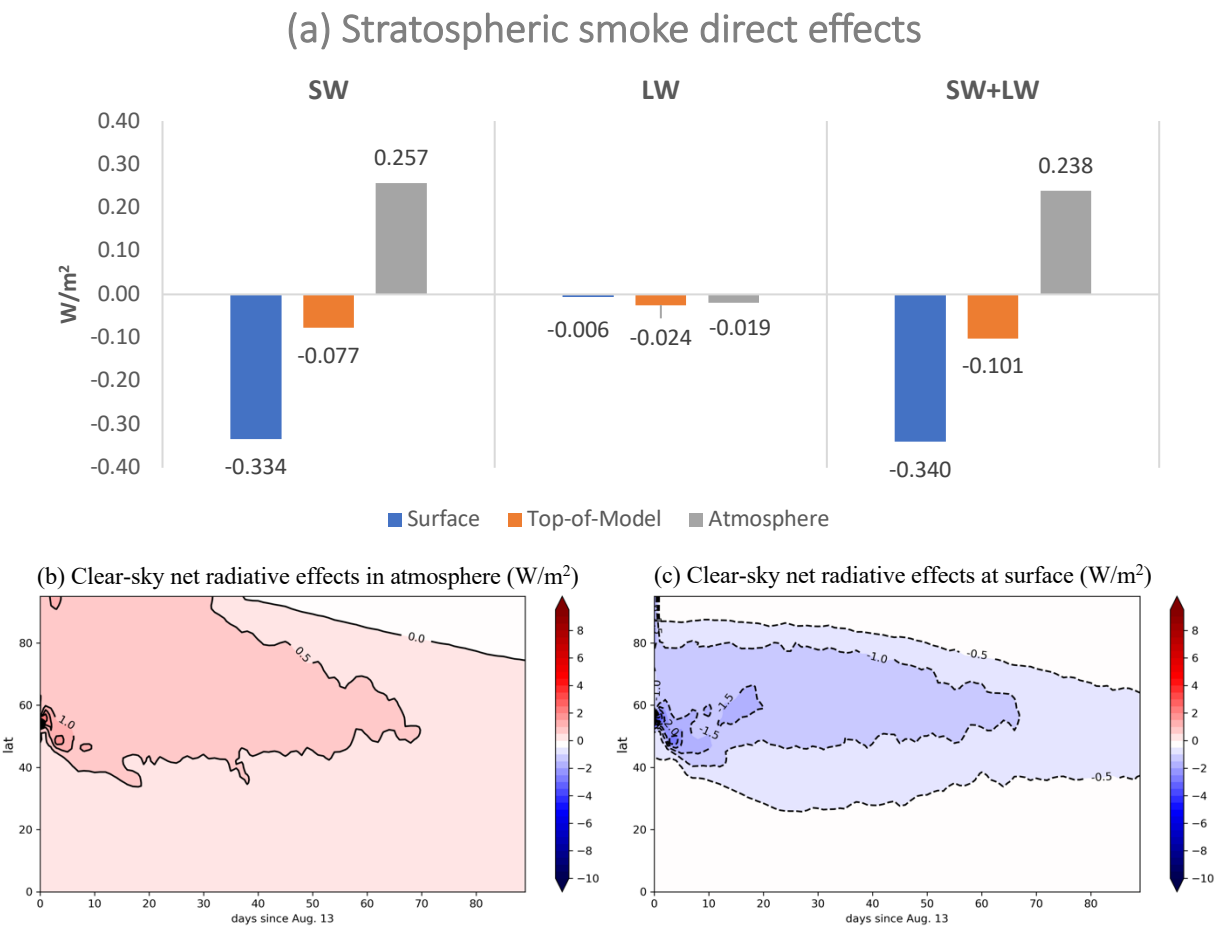

Figure 9. (a) The spatial-temporal averaged radiative effects of simulated smoke aerosols over the northern hemisphere from August 13, 2017 to May 31, 2018. (b) Time series of zonal mean clear-sky net radiative effects of smoke aerosols in atmosphere. (c) The same as (b) but at the surface. Results are from the case 0.2Tg_BC2_13.5km_gamma6.

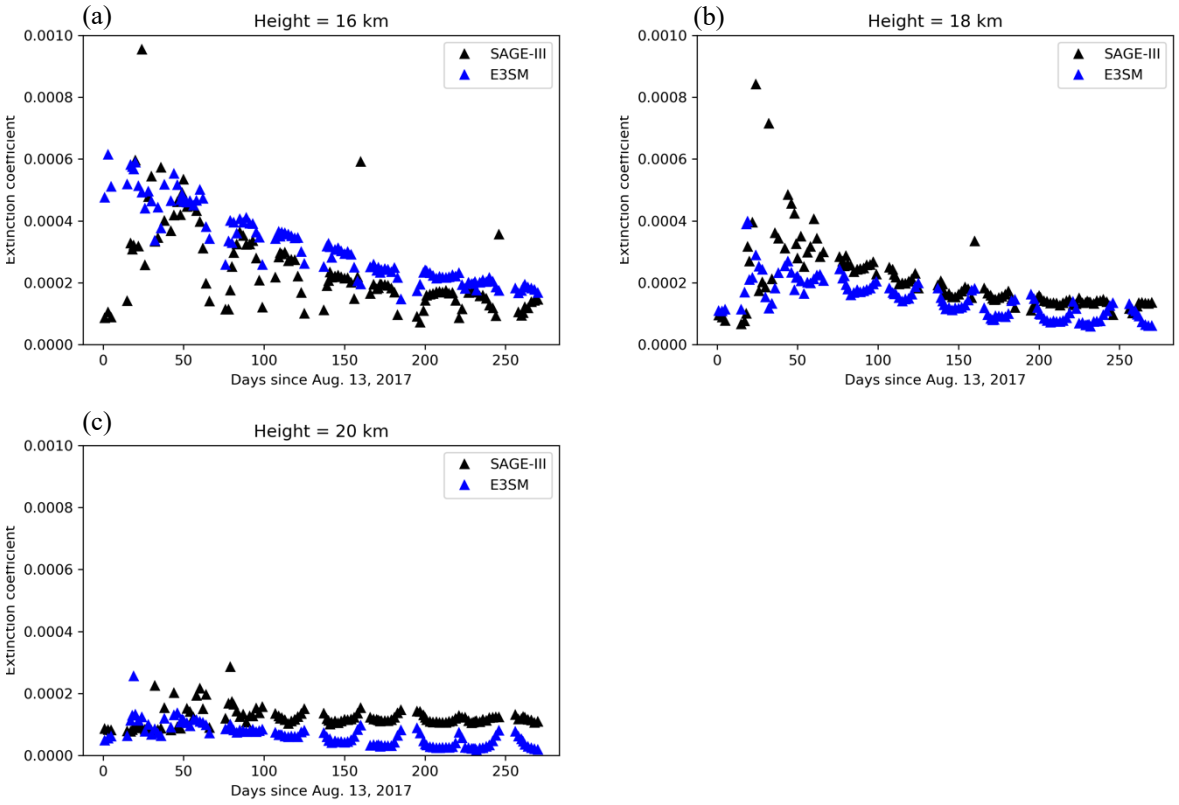

Figure 10. Time series of daily extinction coefficient (1024 nm wavelength; units: km^{-1}) at (a) 16 km, (b) 18 km, and (c) 20 km height. Black triangles the data from SAGE-III, while blue triangles indicate the simulated extinction coefficient from 0.2Tg_BC2_13.5km_gamma6.